KSÜ Mühendislik Bilimleri Dergisi, 26(2), 2023
Araştırma Makalesi

KSU J Eng Sci, 26(2), 2023
Research Article

Kahramanmaras Sutcu Imam University
Journal of Engineering Sciences

Geliş Tarihi : 26.09.2022
Kabul Tarihi : 13.12.2022

Received Date : 26.09.2022
Accepted Date : 13.12.2022

INVESTIGATION OF THE EFFECT OF A DIFFERENT TRAPEZOIDAL INCLINATION ANGLE IN A REVERSE TRAPEZOIDAL CROSS-SECTION FLOW CHANNEL ON THE PERFORMANCE OF THE PEM FUEL CELL WITH THE COMPUTATIONAL FLUID DYNAMIC (CFD) METHOD

TERS TRAPEZ KESİTLİ BİR AKIŞ KANALINDA FARKLI BİR TRAPEZ EĞİM AÇISININ PEM YAKIT PİLİNİN PERFORMANSINA ETKİSİNİN HESAPLAMALI AKIŞKANLAR DİNAMİĞİ (HAD) YÖNTEMİ İLE İNCELENMESİ

Yunus SAYAN[1*] (ORCID: 0000-0002-0871-6842)

[1] Bitlis Eren University, Department of Mechanical Engineering, Bitlis, Türkiye

*Sorumlu Yazar / Corresponding Author: Yunus SAYAN, ysayan@beu.edu.tr

ABSTRACT

In this work, a reverse trapezoidal cross-section channel shape for a single flow channel PEM fuel cell was examined with computational fluid dynamic (CFD) method. ANSYS Fluent was applied to solve electrochemical reactions, potential fields, mass, species, and energy transport equations. Species mass ratio, temperature distribution and relative humidity were obtained for the cell as well as the i-V and power density plots. The results were compared to two reference geometries with the commonly used square section shape for the channel. One reference geometry has the same channel width and height with the reverse trapezoidal cross-section channel while the other has the same cross-section area. The results indicate that the cell with reverse trapezoidal cross sectional flow channel shape has more than 32% higher power density than the cell with square cross-sectional flow channel shapes, but poor water management.

Keywords: PEM fuel cell, channel geometry, modelling, reverse trapezoidal cross-section.

ÖZET

Bu çalışmada, PEM yakıt pilleri için ters yamuk kesitli kanal şekli hesaplamalı akışkanlar dinamiği (HAD) yöntemi ile incelenmiştir. ANSYS Fluent, elektrokimyasal reaksiyonlar, kütle, türler, enerji transferi ve potansiyel alan denklemlerini çözmek için uygulandı. Pillerdeki türlerin kütle oranı, bağıl nem ve sıcaklık dağılımı grafikleri ile polarizasyon ve güç yoğunluğu eğrileri elde edildi. Sonuçlar, PEM yakıt pilleri kanalı için yaygın olarak kullanılan kare kesit şekline sahip iki referans geometri ile karşılaştırıldı. Referans geometrilerinden biri ters yamuk kesitli kanal ile aynı kanal genişliği ve yüksekliğine sahipken, diğeri aynı kesit alanına sahiptir. Analiz sonuçları, ters yamuk kesitli akış kanalı şekline sahip pilin, kare kesitli akış kanalı şekline sahip pilden %32'den daha fazla güç yoğunluğuna sahip olduğunu, ancak su yönetiminin zayıf olduğunu göstermektedir.

Anahtar Kelimeler: PEM yakıt pili, kesit şekli, modelleme, ters yamuk kesit

ToCite: SAYAN, Y., (2023). INVESTIGATION of THE EFFECT of a DIFFERENT TRAPEZOIDAL INCLINATION ANGLE in a REVERSE TRAPEZOIDAL CROSS-SECTION FLOW CHANNEL on the PERFORMANCE of the PEM FUEL CELL WITH THE COMPUTATIONAL FLUID DYNAMIC (CFD) METHOD. *Kahramanmaraş Sütçü İmam Üniversitesi Mühendislik Bilimleri Dergisi*, 26(2), 408-423.

1. INTRODUCTION

Many cities in the world have been suffering from high CO_2 emission and air pollution due to the harmful effect of the fossil fuels. Dependency of fossil fuels has increased in recent years owing to the growing population and industrialization. As a prospective alternative energy solution, fuel cells mitigate internal combustion engine dependency due to high efficient energy generation (Ibrahimoglu, Yilmazoglu, & Celenk, 2017). Among fuel cell variants, proton exchange membrane fuel cells (PEMFCs) are the primary candidates for transportation and portable applications in particular, but also gaining prominence in the stationary/power generation domain, such as in reversible fuel cells (FCs) and electrolyzer systems. (Y. Li, Zhou, Liu, & Wu, 2019).

A fuel cell (FC) is an electrochemical system that efficiently converts chemical potential (from fuel) into electric power (Kerkoub, Benzaoui, Haddad, & Ziari, 2018; Wilberforce et al., 2017). These fuel cells (FCs) can be used for several commercial sources such as laptops, mobile phones, transportation and so on (Awan, Saleem, & Basit, 2018; Kerkoub et al., 2018; Y. Wang, Ruiz Diaz, Chen, Wang, & Adroher, 2020; Zhao & Li, 2019) . PEMFCs can replace conventional fossil fuel-powered devices due to their higher conversion efficiency, relative simplicity, convenient operating temperature, rapid power-up, dynamic load following, silent operation and low emissions (Ibrahimoglu et al., 2017; Kerkoub et al., 2018; Wilberforce et al., 2019). The PEMFC comprises primarily the bipolar plate and the membrane electrode assembly (MEA) as repeating units. The MEA contains a proton exchange membrane (PEM) electrolyte located between two catalysts (electrodes). Each electrodes comprises of a layer of gas diffusion (GDL) and catalyst (Carcadea et al., 2020; Paulino et al., 2017; Wilberforce et al., 2019). The bipolar plate provides reactant gases to reach the MEA for electrochemical reactions as well as removal of products from the MEA. It also provides mechanical support to the cell and works as current collector. The bipolar plates typically consist of different patterns of flow channel grooves in order to deliver reactant gases to both cathode and anode catalyst through the GDLs. It also discharges the produced water carried by diffusion to the channels. Therefore, it is important to design efficient bipolar plate for sufficient reactants' supply and products' removal. Efficient bipolar design also results in an overall improved fuel cell performance alongside power density generation. It would accrue further benefits in terms of homogenous reactant and product transport, such as a more uniform electrochemical active area (lower prospect of starvation or flooding), optimal thermal distribution (mitigation of thermal runaway, hotspots) and potentially improved durability and ruggedness (Paulino et al., 2017).

There have been many studies performed regarding to the investigation of the channel designs on the PEMFC's performance comprising serpentine channels (single as well as multiple), parallel channels and interdigitated channels (Kerkoub et al., 2018). Channel dimensions (depth, width) and flow field patterns are important design parameters for the PEMFC's operation owing to their high influence on the durability and performance. Better heat and water management, a sufficient distribution of reacting species on catalysts and minimization of the pressure loss are a few critical problems that should be handled by the optimization of flow field (Carcadea et al., 2021). Four distinct channel geometries (serpentine zig-zag, straight zig-zag, serpentine parallel and straight parallel) were studied by Saco et al. (Arun Saco, Thundil Karuppa Raj, & Karthikeyan, 2016) with a rectangular configuration. According to their result, the better current and power densities were obtained from the straight zig-zag flow channels. Yi et al. (Yi & Van Nguyen, 1999) studied the influence of different flow channel geometries on the PEM fuel cell efficiency, reporting better cell performance with an interdigitated configuration. Lim et al. devised an altered parallel flow field in order to overturn an uneven dispersal of reactants and product in the parallel channels feature (Lim, Majlan, Daud, Rosli, & Husaini, 2020). They report that the cell efficiency enhanced as a result of improved transport of reacting gases to corresponding active sites and discharge of excessive water. The design of step-wise depth for the parallel flow channel was investigated by Ferng et al. (Ferng & Su, 2007). They found that this design improved substantially the PEMFC's performance. The channels' cross sectional areas including width of ribs, height and width of the channels have been of interest to many other researchers (Kerkoub et al., 2018). They examined these parameters for different designs so as to obtain better cell performance and flow management. Manso et al. reported that the aspect ratio of the channel cross-section has considerable influence on the power output behavior of the PEMFC at low polarization (Manso, Marzo, Mujika, Barranco, & Lorenzo, 2011). Different shapes of cathode channel were examined by Wang et al.(X. D. Wang, Lu, Duan, & Lee, 2012). According to their result, the cell with triangular cross-sectional channel showed superior characteristics to the cell with rectangular cross-sectional channel at low operating voltage. In addition, there are several studies that have examined the effect of flow channel cross-sectional profiles on PEMFC operating behavior (triangular, rectangular, trapezoidal and curved) (Carcadea et al., 2021). Li et al studied different flow channel cross-sectional profiles on the PEMFC's performance (C. Li, Xu, Hu, Mei, & Yang, 2021). They reported that the cell possessing a triangular cross-sectional flow channel has greater

current density (for the same operating voltage) compared to the cell using trapezoidal cross-section flow channels. Paulino et all (Paulino et al., 2017) also studied different cross-sections of the flow channel on the PEMFC's performance. According to their result, the cell with rectangular cross-sectional channel generated better current density in comparison to the cell with trapezoidal cross-sectional channel.

Despite many research works carried out and published on the devise of the flow field geometry, the full unlocking of the effects of various flow channel cross section shapes on the PEM fuel cell is still a work-in-progress. This problem is uncertain about which flow field geometry are more promising and appropriate for the future development of the PEMFCs.

In this paper, a reverse trapezoidal cross-section channel shape for PEM fuel cells was investigated. In order to examine holistically the influence of the cross-sectional shape on the performance of the cell, the authors constructed and applied a three dimensional computational fluid dynamic (CFD) model by utilizing ANSYS Fluent Fuel Cells Module. Initially, two single channel cells with square cross-section flow channel (having different cross-sectional area) were analyzed as references. Later, a single channel cell with a reverse trapezoidal cross-section flow channel was simulated under the same operating conditions. Their results were compared with each other in terms of species consumption, water formation, relative humidity, temperature distribution and performance.

PEM FC MODELING

Numerical Modeling

PEM fuel cells are multiphysics systems, thus many processes occur that describe their operation, encompassing: (i) mass transport of gaseous and liquid molecules/species (O_2, N_2 and H_2O vapor/liquid on the cathode; H_2 gas and H_2O vapor/liquid on the anode) associated with fluid flow (ii) electrochemical reactions and (iii) heat transfer. To model these processes numerically, differential equations defining mass, momentum, electric charges, and energy conservation are needed.

Here, ANSYS Fluent was used to model and simulate a 3-D single-channel PEMFC possessing different cross-sectional profiles. The following conditions were assumed for the model: flow is incompressible and laminar; the model is computed for a steady state condition of the system; gravitational effects are ignored; the catalyst layers (CLs), gas diffusion layers (GDLs) and electrolyte are homogeneous and isotropic; gases are ideal; water phase change is not considered; there is no gas diffusion throughout electrolyte.

The governing equations describing the model are used to simulate and analyze multiphase flow, temperature and current density in the PEMFC. They are given as follows:

- ***Conservation of mass equation***

$$\frac{d\rho}{dt} + \nabla.(\rho v) = S_m \quad (1)$$

$$S_m = -\frac{M_{H_2}}{2F} J_a - \frac{M_{H_2O}}{F} J_a \quad \text{for hydrogen} \quad (2)$$

$$S_m = -\frac{M_{O_2}}{4F} J_c - \frac{M_{H_2O}}{2F} J_c \quad \text{for oxygen} \quad (3)$$

Where ρ, t, v, S_m, M_{H2}, M_{O2}, M_{H2O} *and* F are the density (kg m^{-3}), time (s), velocity (m s^{-1}), mass source term (kg m^{-3} s^{-1}), molar mass of hydrogen (kg mol^{-1}), molar mass of oxygen (kg mol^{-1}), molar mass of water (kg mol^{-1}), *and* Faraday's constant (C kg^{-1}mol^{-1}), respectively. In addition, J_c and J_a are the exchange current densities (A m^{-2}) at the cathode and anode, respectively.

- ***Butler-Volmer equation***

$$J_a = \left(A_{\mathrm{a}} i_{\mathrm{a}}^{ref}\right)\left(\frac{C_{H_2}}{C_{H_2}^{ref}}\right)^{\gamma_{\mathrm{a}}}\left[e^{\frac{\alpha_{\mathrm{a}} F\,\eta_{\mathrm{a}}}{RT}} - e^{\frac{-\alpha_{\mathrm{c}} F\,\eta_{\mathrm{a}}}{RT}}\right] \quad (4)$$

$$\eta_a = \varphi_{solid} - \varphi_{membrane} \quad (5)$$

$$J_c = \left(A_c i_c^{ref}\right)\left(\frac{C_{O_2}}{C_{O_2}^{ref}}\right)^{\gamma_c}\left[-e^{\frac{\alpha_{\mathrm{a}} F\,\eta_c}{RT}} + e^{\frac{-\alpha_{\mathrm{c}} F\,\eta_c}{RT}}\right] \quad (6)$$

$$\eta_c = \varphi_{solid} - \varphi_{membrane} - V_o \quad (7)$$

Where *a* and *c* subscripts denote the anode and cathode, respectively. Furthermore, *A, i, ɣ, a, R, T, η, φ, V_o, C* and C^{ref} are the specific active surface area (m^{-1}), reference current density (Am^{-2}), concentration dependence, charge transfer coefficient, universal gas constant ($J\ K^{-1}\ mol^{-1}$), temperature (K), activation losses (V), potential (V), open circuit voltage, local species concentration and reference value ($kg\ mol\ m^{-3}$), respectively.

- ***Conservation of momentum equation***

$$\nabla.\left(\varepsilon\rho\vec{\boldsymbol{u}}\vec{\boldsymbol{u}}\right) + \varepsilon\nabla P - \nabla.\left(\varepsilon\mu\nabla\vec{\boldsymbol{u}}\right) + \frac{\mu\varepsilon^2\vec{\boldsymbol{u}}}{K} = 0 \quad (8)$$

Where *u, ε, P, μ* and *K* are the velocity vector ($m\ s^{-1}$), porosity, pressure (Pa), dynamic viscosity ($kg\ m^{-1}\ s^{-1}$) and permeability (m^2), respectively.

- ***Gas reactant equation***

$$\nabla(\rho_i\vec{\boldsymbol{u}}_i Y_i) = \nabla\left(\rho_i D_i^{ef}\nabla Y_i\right) + S_i \quad (9)$$

Where *i* represents H_2, O_2, N_2 and H_20, *Y* denotes mass fraction, *S* denotes the source term and D^{ef} is the effective mass diffusivity (m^2s^{-1})

- ***Liquid water equation***

$$\nabla(\rho_l\vec{\boldsymbol{u}}_l f) = \nabla(\rho_l D_l\nabla Y\varphi_l) + S_l \quad (10)$$

Where *l* represents the liquid, *f* is the interfacial drag coefficient, *D* is the mass diffusivity (m^2s^{-1}) and *φ* is the potential (V).

- ***Water equation in membrane***

$$\frac{\rho_{mem}}{ZW}\nabla\left(D_d^{ef}\nabla\lambda_d\right) + S_d = 0 \quad (11)$$

Where *ZW* is the gram equivalent of electrolyte ($kg\ kmol^{-1}$), *d* describes dissolved water and *λ* is the water content in lame constant or ionomer.

- ***Conservation of energy***

$$\nabla.(\rho v H_T) = k_{ef}\nabla.(\nabla T) + S_T \quad (12)$$

$$S_T = I^2 R_{ohm} + h_{react} + \eta_{act} R_{a/c} \quad (13)$$

Where H_T, k_{ef}, S_T, I, R, h *and* η are the total enthalpy (J mol^{-1}), effective thermal conductivity (W m^{-1} K^{-1}), source term of energy (W m^{-3}), current (A), resistivity of conducting media (ohm), net enthalpy change (J mol^{-1}) and activation over potential (V), respectively.

- ***Ohmic's law for electron and protonic transport***

$$\nabla.(\sigma\nabla\Phi) + R = 0 \tag{14}$$

Where σ, Φ and R are the electrical conductivity (1/ohm m), electrical potential (volts) and volumetric transfer current (A m^{-3}), respectively.

Geometrical Modeling

In the present paper, two different flow channel geometries were considered for the PEMFC performance investigation. From top to bottom, the components are: bipolar plate; anode gas flow channel (GFC); anode gas diffusion layer (GDL); membrane electrode assembly (MEA) (anode catalyst, electrolyte and cathode catalyst); cathode gas diffusion layer; cathode gas flow channel; bipolar plate. One flow channel geometry has a square cross-section with two different dimension (cell 1 and cell 2). Other flow channel geometry has a reverse trapezoidal cross-section (cell 3). These cells are identical, and they only differ from each other by the cross-section of their flow channel. The cross-section shapes of cell 1 and cell 2 are the same but they have the different cross-sectional area. Moreover, the cross sectional shape of cell 3 is different than that of cell 2 and cell 1. However, the cross-sectional area of cell 2 and cell 3 is the same. Cells were constructed as single-channel PEMFCs with 40 mm length. A representation view of the constructed models is displayed in Figure 1 with detailed channel cross-sections. The geometric details of the PEMFC can be seen in Table 1 and Figure 1.

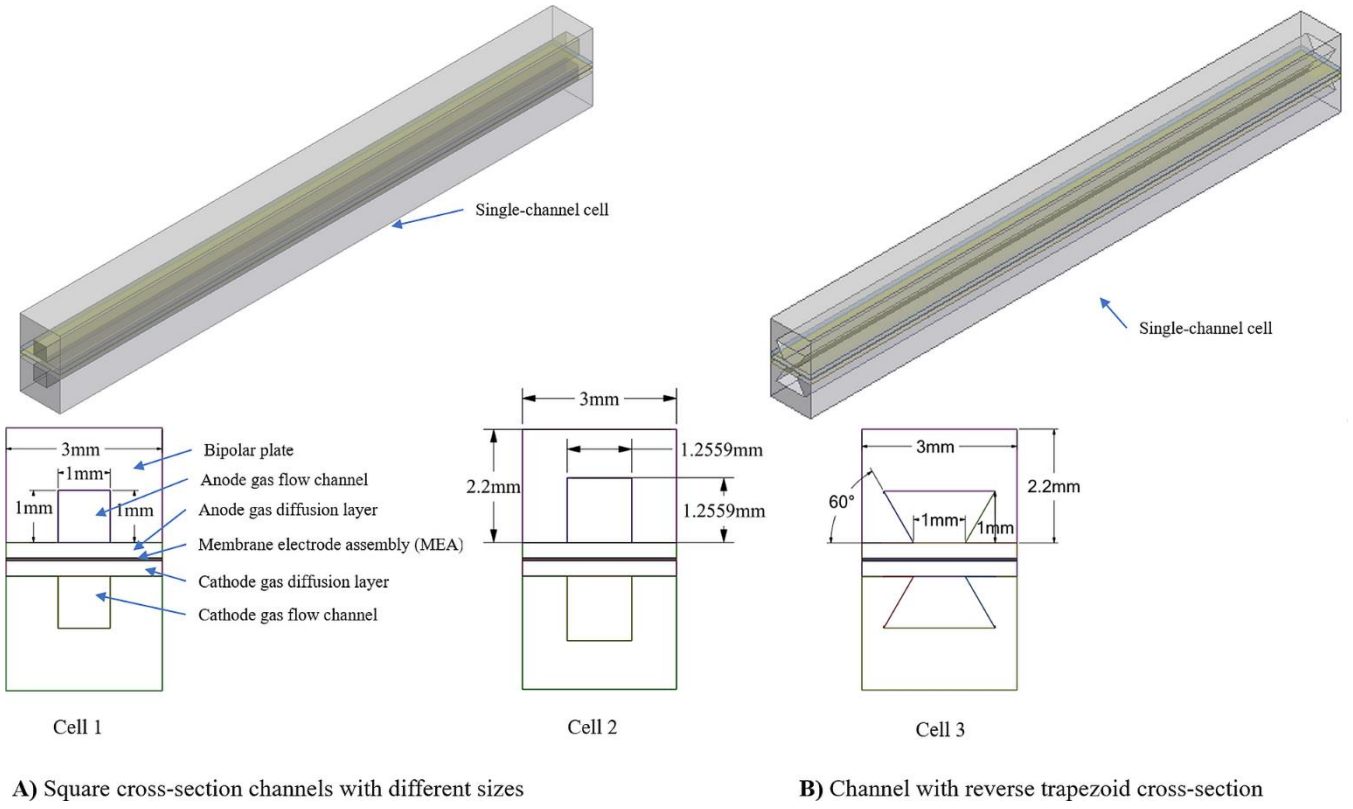


Figure 1. A Representation View of the Constructed Models with Detailed Channel Cross-Sections

In order to gauge the impact of gas channel geometries on PEMFC, two flow channels with a square cross-section and a flow channel with an inverted-trapezoidal cross-section were designed for a single channel cell. The square or rectangular cross-section channels are extensively used for PEMFCs. Therefore, they are being considered as reference compared to other geometries. Cell 1 and cell 3 possess the same flow channel height and bottom edge width but different top edge width (different cross-section shape). Therefore, their flow channel has different cross-

section area. As is well known, changing the cross-sectional area will affect the velocity of the flow through that section for a given mass flow rate. To properly analyze and quantify the effect of the flow channel geometry independently, a model (cell 2) with the same flow channel cross-section area of cell 3 was designed. Thus, cell 2 and cell 3 have the same cross-sectional area of their flow channels but different shapes. Lastly, cell 1 and cell 2s' flow channels possess the same cross-section shape but different size.

In this work, the purpose of using reverse trapezoidal cross section for fuel cell gas channel is to promote the cell's overall performance characteristics deriving from better velocity management of species due to a unique shape.

Table 1. Geometric Properties of the PEMFC Model Employed in the Study

Quantity	**Value**
Thickness of the bipolar (mm)	2.2
Width of the channel (mm)	1
Height of channel (mm)	1
Length of the channel (mm)	40
Thickness of the anode gas diffusion (gdl)(mm)	0.3
Thickness of the anode catalyst (cl)(mm)	0.01
Thickness of the membrane (mm)	0.03
Thickness of the cathode catalyst (cl)(mm)	0.01
Thickness of the cathode gas diffusion (gdl)(mm)	0.3
Total reaction area (mm^2)	120

Operating Parameters

In this study, three single channel cells which have a total reaction area of 120 mm^2 were analyzed under the same operating settings. The operating temperature and pressure were set to be 80 ºC and 101325 Pa, respectively. The operating conditions and input parameters set in this research are provided in Table 2.

Table 2. Operating Conditions and Some of the Input Parameters Used in the Numerical Simulations.

Parameter	Value
Operating pressure (Pa)	101325
Operating temperature (K)	353.15
Osmotic drag source	1
Open circuit voltage (V)	1.22
Anode reference current density (A m^{-2})	10000
Cathode reference current density (A m^{-2})	10
Anode gas diffusion layer porosity	0.6
Gas diffusion layer permeability of the anode (m^2)	3e-12
Anode catalyst layer porosity	0.2
Anode catalyst layer permeability (m^2)	2e-13
Catalyst layer surface volume ratio of the anode (1/m)	200000
Electrolyte equivalent weight (kg $kmol^{-1}$)	1100
Electrolyte protonic conduction coefficient	1
Electrolyte protonic conduction exponent	1
Electrolyte water diffusivity coefficient	1
Cathode gas diffusion layer porosity	0.6
Cathode gas diffusion layer permeability (m^2)	3e-12
Cathode catalyst layer porosity	0.2
Cathode catalyst layer permeability (m^2)	2e-13
Catalyst layer surface volume ratio of the cathode (1/m)	200000
Cathode ionomer resistance (s m^{-1})	100
Anode porous jump resistivity (ohm m^{-2})	2e-6
Cathode porous jump resistivity (ohm m^{-2})	2e-6
Inlet mass flow rate of the anode(kg s^{-1})	4e-7
Inlet and outlet temperature of the anode (K)	353.13
Inlet H_2 mass fraction of the anode	0.6
Inlet H_2O mass fraction of the anode	0.4
Inlet mass flow rate of the cathode(kg s^{-1})	3e-6
Inlet and outlet temperature of the cathode (K)	353.13
Inlet O_2 mass fraction of the cathode	0.21
Inlet H_2O mass fraction of the cathode	0.15
Anode terminal electric potential (V)	0
Cathode terminal electric potential (V)	0.9, 0.85, 0.80, 0.75, …0.2
Electrolyte (Nafion) (density kg m^{-3})	1980
Electrolyte (Nafion) thermal conductivity (W $m^{-1}K^{-1}$)	2
Electrolyte (Nafion) electrical conductivity (S m^{-1})	1e-16
Electrolyte (Nafion) specific heat (J kg^{-1} K^{-1})	2000
Bipolar plate (aluminum) density (kg m^{-3})	2719
Bipolar plate (aluminum) specific heat (J $kg^{-1}K^{-1}$)	871
Bipolar plate (aluminum) thermal conductivity (W $m^{-1}K^{-1}$)	100
Bipolar plate (aluminum) electrical conductivity (S m^{-1})	1000000
Anode and cathode catalyst (Graphite+Pt) density (kg m^{-3})	2719
Anode and cathode catalyst (Graphite+Pt) specific heat (J $kg^{-1}K^{-1}$)	871
Anode and cathode catalyst (Graphite+Pt) thermal conductivity (W $m^{-1}K^{-1}$)	10
Anode and cathode catalyst (Graphite+Pt) electrical conductivity (S m^{-1})	5000
Anode and cathode gas diffusion layer (Graphite) density (kg m^{-3})	2719
Anode and cathode gas diffusion layer (Graphite) specific heat (J kg^{-1} K^{-1})	871
Anode and cathode gas diffusion layer (Graphite) thermal conductivity (W m^{-1} K^{-1})	10
Anode and cathode gas diffusion layer (Graphite) electrical conductivity (S m^{-1})	5000

Mesh Validation

Mesh generation directly influences the time for simulation and its results. In order to gain confidence in the validity of the simulation, it is standard practice in the CFD workflow to prepare the model meshing which must first establish grid independence i.e. a set of results invariant or independent of mesh size. Therefore, current densities of the cell 2 were calculated by ANSYS Workbench at five different number of elements at a constant operating voltage of 0.5 V. The mesh density was increased from 657200 to 2959479 elements as shown in Table 3. The results display that increasing the number of elements has little effects on current density of cell 2 (see Table 3 and Figure 2). The cell current density decreased by %0.5 when the number of element increased from 657200 to 2959479. This margin of

error can be tolerated, as the increase in the number of elements will significantly increase the analysis time. Therefore, the number of elements were chosen to be around 657200 for the all other analyses in this study.

Table 3. Current Density Changes of Cell 2 at Different Number of Elements at A Constant Operating Voltage of 0.5 V

Order	Elements' number	Voltage (V)	Current density (W cm^{-2})	Current density change %
1	657200	0.5	1.295	
2	860472	0.5	1.2919	0.239956653
3	1270300	0.5	1.2934	0.115973403
4	1792369	0.5	1.2854	0.622374358
5	2959479	0.5	1.2887	0.256072011

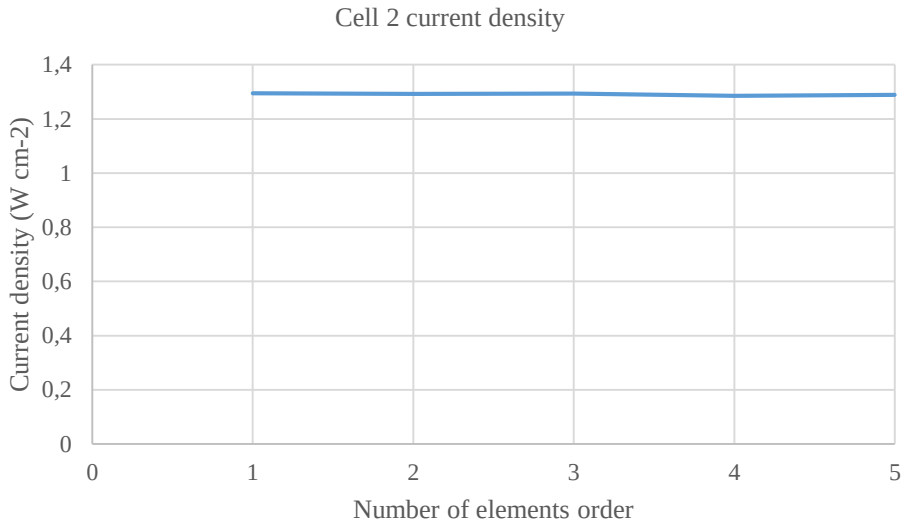


Figure 2. Current Density Changes of the Cell 2 at Different Number of Elements at A Constant Operating Voltage of 0.5 V

RESULTS AND DISCUSSION

Figure 3 depicts cross sectional view of the velocity distribution of the single channel cell 1, cell 2 and cell 3 at the middle of the cells in the flow direction and in the transverse direction. The maximum flow rate occurs along the mid-axis length of the channels for all cells. In addition, the flow velocity of the gases starts at low speeds at the anode and cathode channels' inlets and increases towards outlets of electrodes' channels. When the maximum gas flow rates occurring in the cells are compared with each other, the maximum flow rate occurs in the gas flow channels of the cell 1 (cross-sectional area of 1 mm^{-2}) as 7.16 m s^{-1}. This is an expected phenomenon, since for the same mass flow rate, the normal flow velocity is higher in the channel with a smaller cross-sectional area. This can be explained by the law of conservation of mass. However, for the same flow channel cross-sectional area (cell 2 and cell 3 with a cross-section area of 1.577 mm^{-2}) and mass flow rate, maximum gas velocity occurs within channels of cell 2 as 4.61 m s^{-1}. The reduced velocity (2.39 m s^{-1}) in flow channels of cell 3 can be explained by the inverse trapezoidal cross-sectional shape.

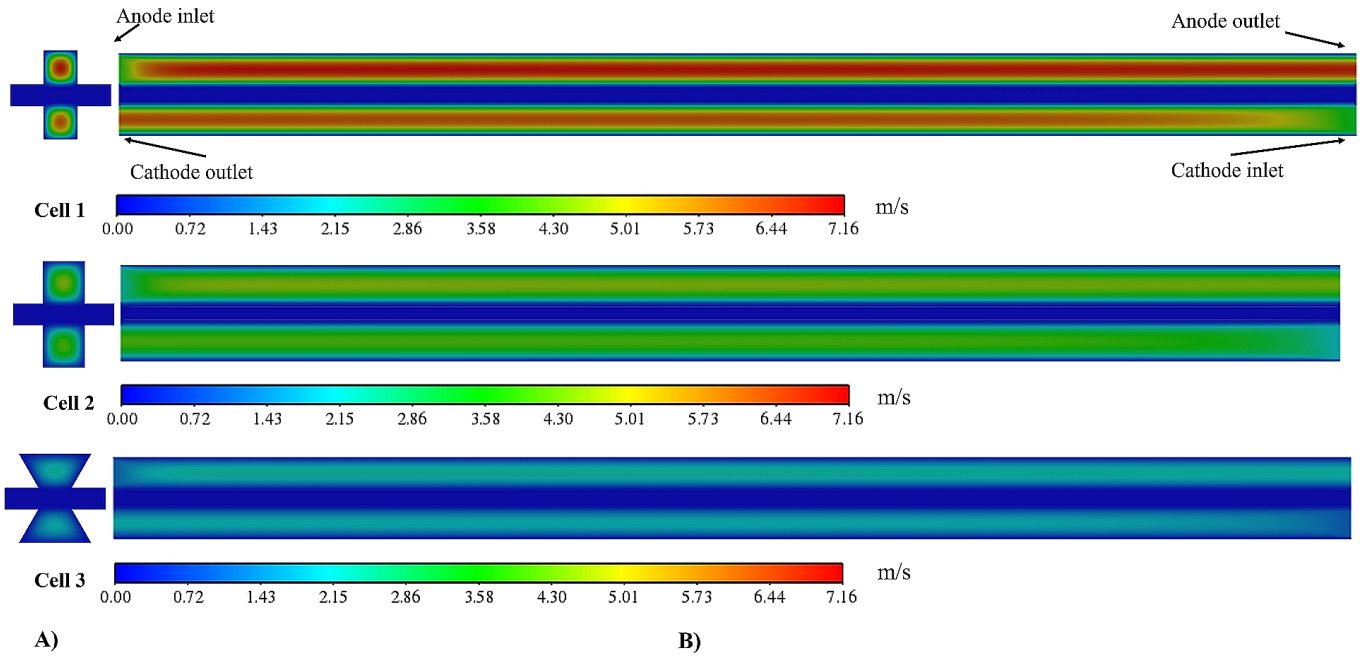


Figure 3. Cross Sectional View of the Velocity Distribution of the Cells at the Middle of the Cells Operating at 0.55 V **A.** in the Flow Direction and **B.** in the Transverse Direction

Cross sectional view of H_2 mass fraction distribution of the single channel cell 1, cell 2 and cell 3 at the center of the cells in the transverse direction at cell voltage of 0.55 V is shown in Figure 4. H_2 mas fraction decreases from anode flow channel inlet to outlet for all the cells as expected. Maximum mass fraction of H_2 is around 0.48 for cell 1 and cell 2, while it is around 0.42 for cell 3 at the outlet of the anode gas flow channel. Figure 5 illustrates the O_2 mass fraction at the same cross-sectional view. As can be seen, the mass fraction of O_2 diminishes from cathode flow channel inlet to outlet for cell 1, cell 2 and cell 3. Oxygen gas depletion becomes more dominant in the cathode gas flow channel outlet of the cell 3 in comparison to cell 1 and cell 2 (bigger green area at the cathode outlet of cell 3 in Figure 5). The reason why the hydrogen gas ratio at the anode channel outlet and the oxygen gas ratio at the cathode channel outlet in cell 3 is less than that of cell 1 and cell 2 can be explained as follows: A better electrochemical reaction might have occurred in cell 3 compared to cell 1 and cell 2. This might be because species with a lower flow rate have enough time to undergo an electrochemical reaction on the catalysts. Following the improved electrochemical activity, the amount of reactant through flow channel decreases. This also improves the fuel efficiency. It is also expected to increase fuel cell performance.

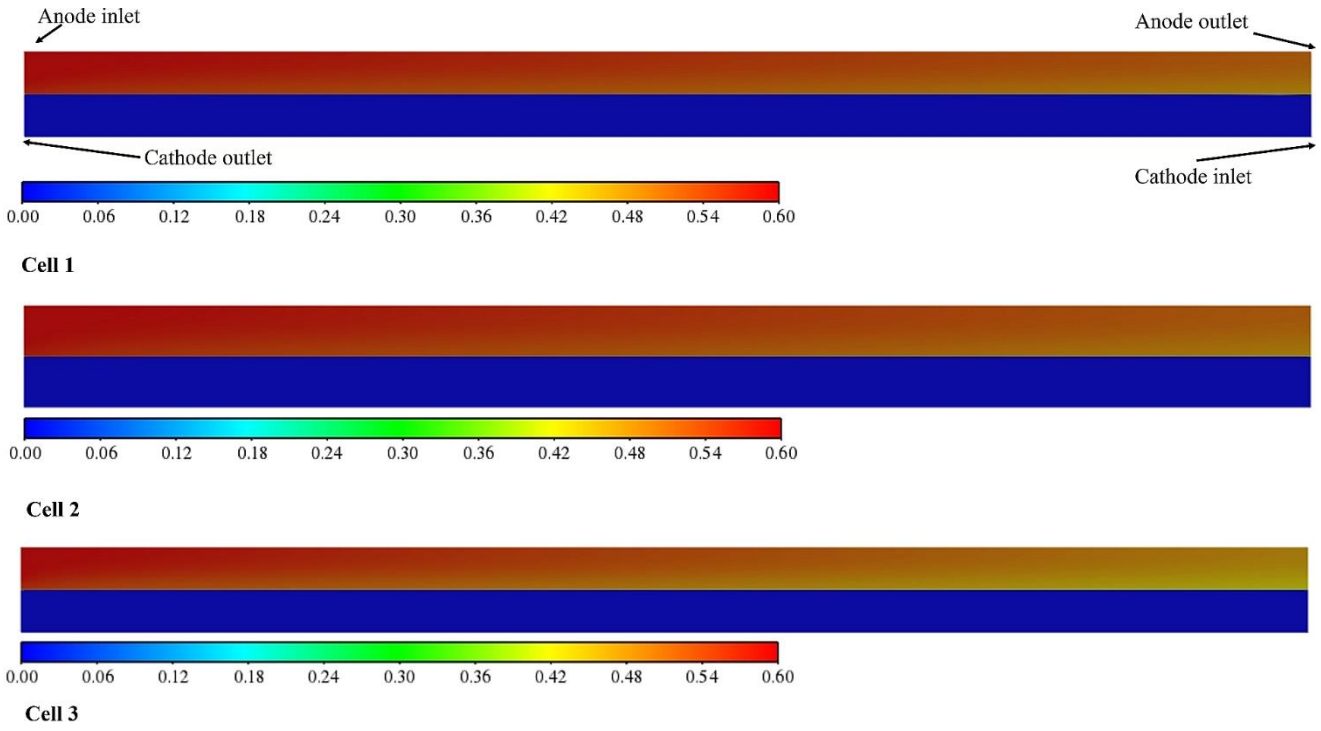


Figure 4. Cross Sectional View of the H_2 Mass Fraction Distribution of the Cells at the Center of the Cells Shown in the Transverse Direction at an Operating Voltage of 0.55 V.

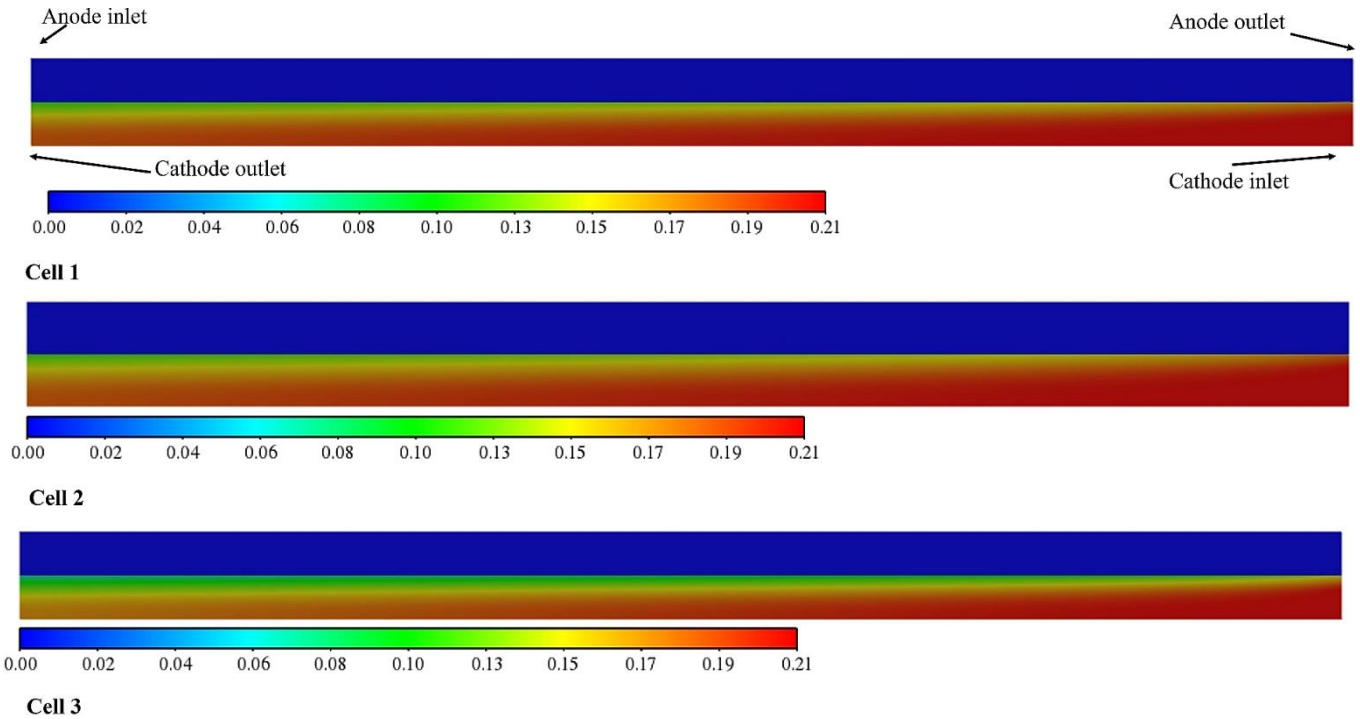


Figure 5. Cross Sectional View of O_2 Mass Fraction Distribution of the Cell 1, Cell 2 And Cell 3 at the Middle of the Cells Shown in the Transverse Direction at an Operating Voltage of 0.55 V.

In PEMFCs, a water balance is required to obtain the optimal performance (Jourdani & Mounir, 2015). The protons (H^+) generated at the anode electrode need water molecules to flow from anode to cathode through electrolyte by the electro-osmotic drag. Thus, the membrane electrolyte needs water so as to have good protonic conductivity (Carcadea et al., 2021). Lack of humidity in the gas channels brings about the condition whereby the membrane interface lose water. This causes a decrease in the effective protonic conductivity of the membrane (increased ohmic electrolyte resistance).(Jourdani & Mounir, 2015). However, if water content is too high, flooding results (Wilberforce et al.,

2017). Excessive water in the cell blocks gas diffusion layer and catalyst pores, impeding the diffusion of species and therefore the polarization related to mass transport and concentration gradients increases. In addition, excessive water in catalyst covers the active surface areas where electrochemical reactions occur and thus leads to cell's performance drop (Penga, Tolj, & Barbir, 2016; (Arif, Cheung, & Andrews, 2022). The membrane optimal relative humidity is required to be between 80% to 100% (Jourdani & Mounir, 2015). The water generation rate in cells depends on current generation rate. With increased current loads (i.e. large current densities) , the production of water in cell is higher (Arif et al., 2022).

It is important to have a good flow channel design for effective flow control and hence better cell performance. Figure 6 shows cross sectional view of H_2O molar concentration distribution of the single channel cells across the central plane of the cells in the transverse direction at an operating voltage of 0.55 V. In addition, Figure 7 illustrates relative humidity in all cells at the same cross-sectional view. It is clear that maximum H_20 concentration and relative humidity in all cells occur at the cathode outlets as expected. Maximum molar concentration of H_20, was obtained in cell 1 and cell 2 as 0.012 kmol m^{-3} and 0.0119 kmol m^{-3}, respectively. They are almost the same. However, the maximum molar concentration of H_20 in cell 3 was obtained as 0.0249 kmol m^{-3}. In addition, maximum relative humidity was around %73 in cell 1 and cell 2 while it is around %150 in cell 3 at an operating voltage of 0.55 V. These results show that, cell 3 generates more current density than cell 1 and cell 2 as can be seen in Figure 9. However, relative humidity in cell 3 is quite high (%150), which could block pores and catalyst active surface areas.

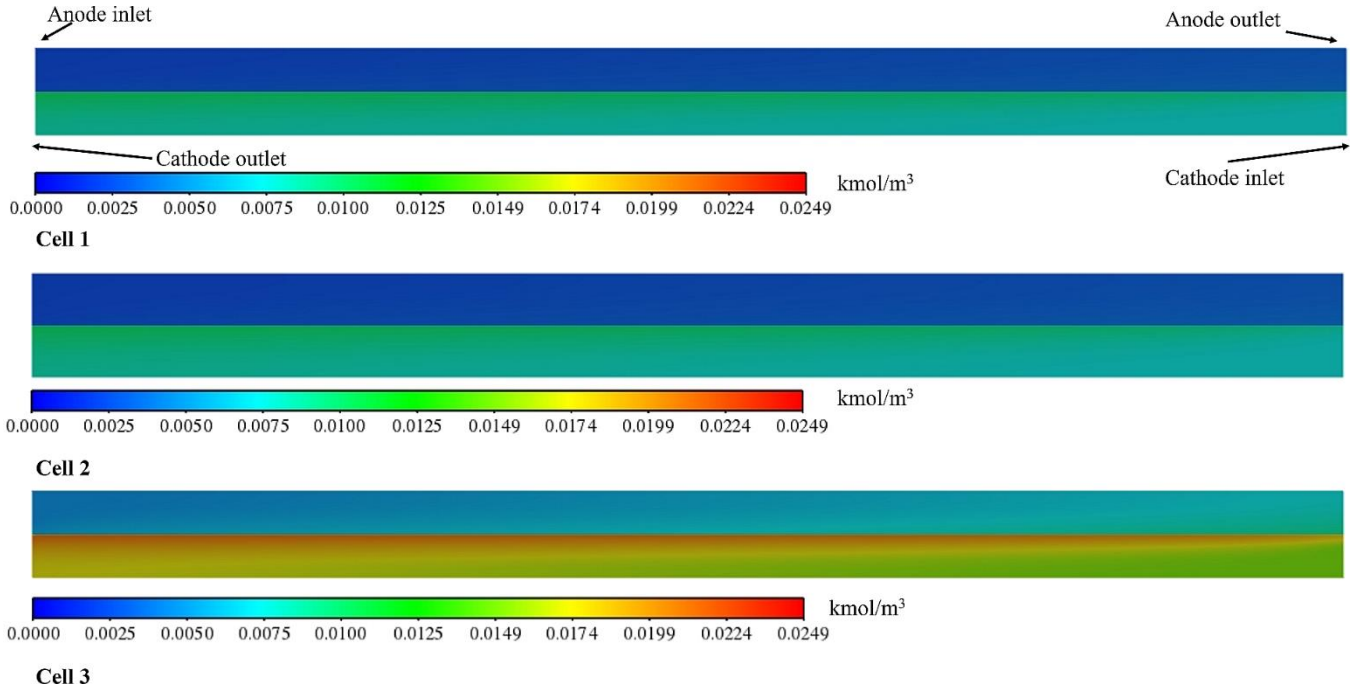


Figure 6. Cross Sectional View of H_2O Molar Concentration Distribution of the Cell 1, Cell 2 And Cell 3 at the Middle of the Cells Shown in the Transverse Direction at an Operating Voltage of 0.55 V.

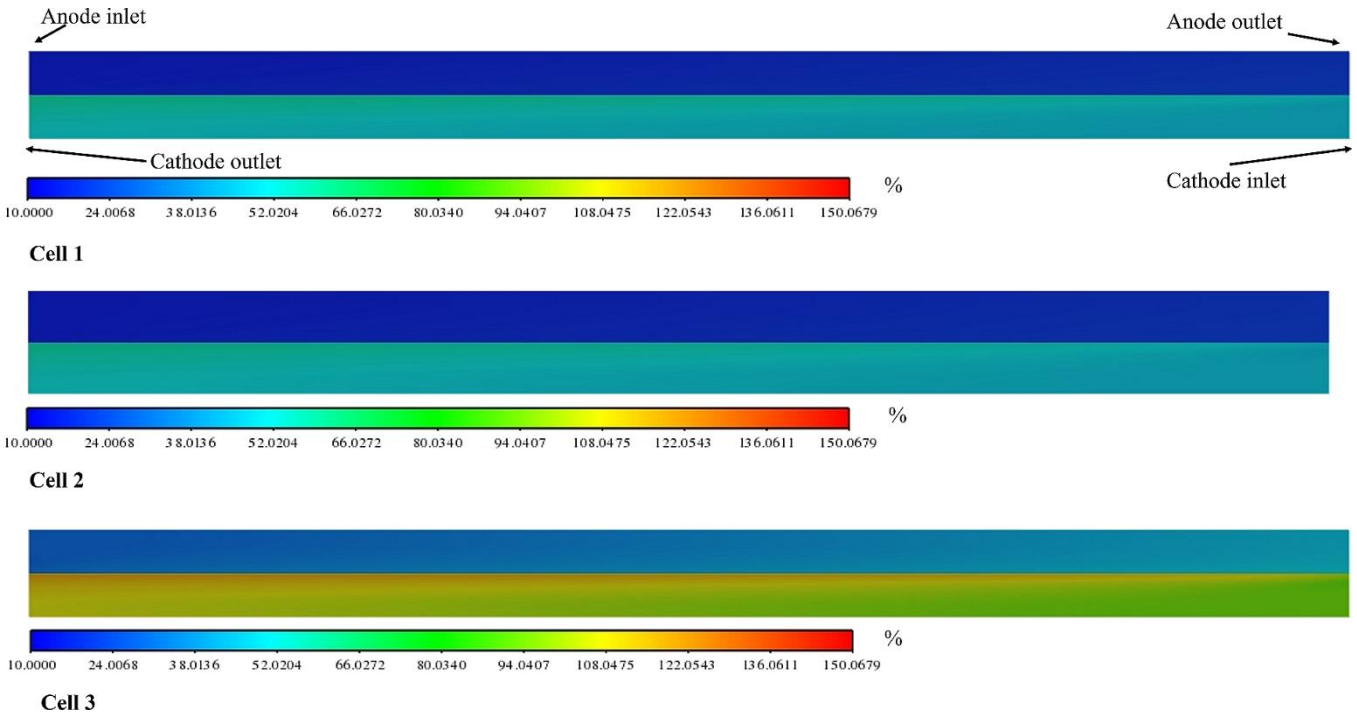


Figure 7. Cross Sectional View of Relative Humidity Distribution of the Cell 1, Cell 2 and Cell 3 at the Middle of the Cells Shown in the Transverse Direction at an Operating Voltage of 0.55 V.

Figure 8 shows temperature distribution of the single channel cells at the same cross sectional view mentioned above paragraphs. The working temperature and condition of these cell were set to be 80ºC and isothermal, respectively. However, temperature of the all cells increased a couple of degree. The temperature distribution of cell 1 and cell 2 is almost uniform, but that of cell 3 is not uniform. The maximum temperature was obtained in cell 3 as about 84 ºC while the maximum temperature in cell 1 was obtained as around 82ºC. According to this figure, there is a small temperature gradient in all cells. The maximum temperature gradient among these cells occurred as 4ºC in cell 3. It must be taken into account since this temperature difference could cause thermal stresses in the cell.

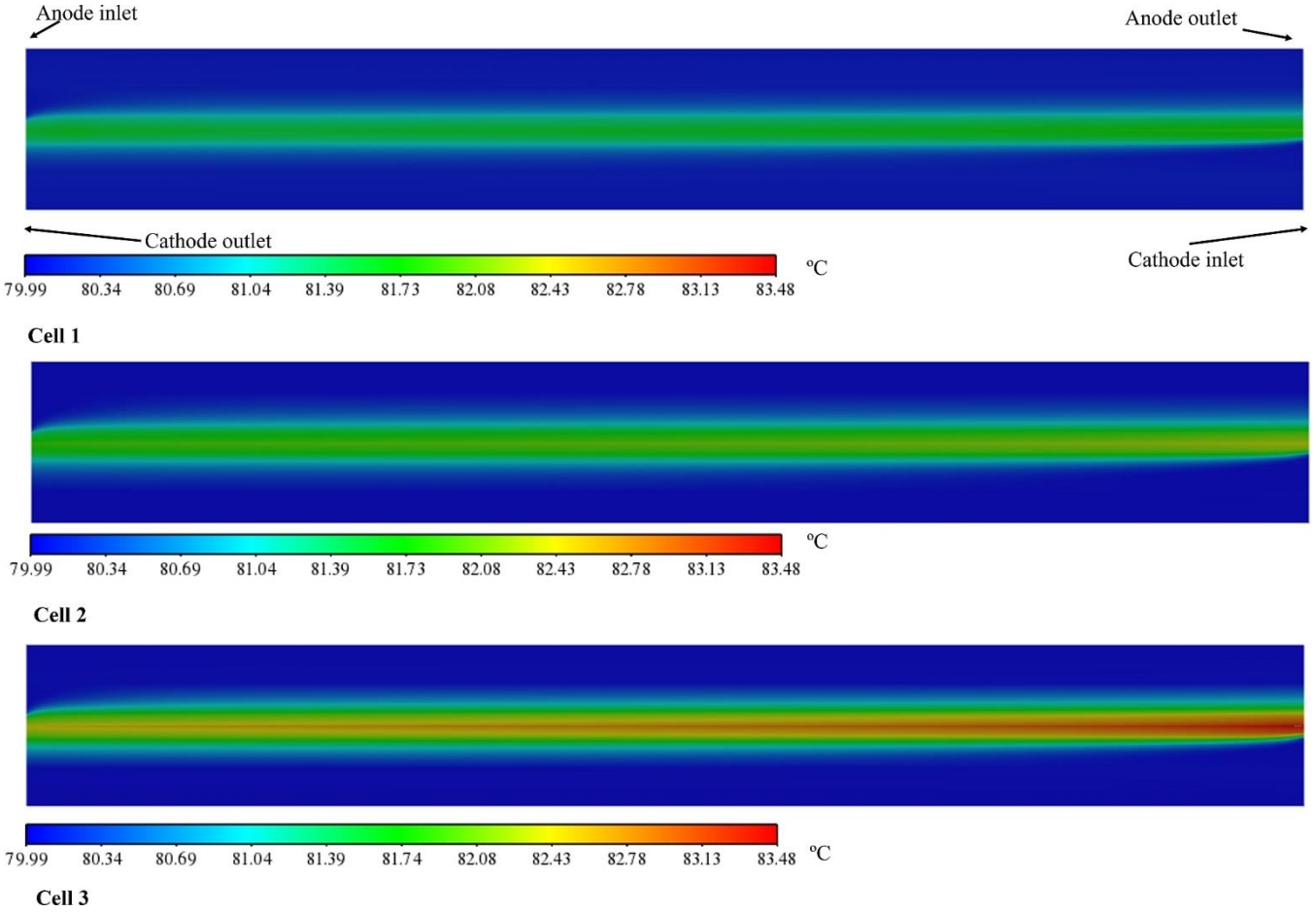


Figure 8. Cross Sectional View of Temperature Distribution of the Cell 1, Cell 2 And Cell 3 at the Center of the Cells Shown in the Transverse Direction at an Operating Voltage of 0.55 V.

In order to obtain polarization curves of these cells, all cells were simulated at different operating voltages ranging 0.9 V as the initial maximum, to 0.2 V by 0.05 V decrements. The obtained results are plotted in Figure 9. Maximum power density was achieved from cell 3 as 0.944185 W cm^{-2} at an operating voltage of 0.55 V. At the same operating voltage and working conditions, the power density of cell 1 and cell 2 were acquired as 0.68178 W cm^{-2} and 0.71225 W cm^{-2}, respectively. It is apparent that the reverse trapezoidal cross-section of the cell 3's flow channel led to a substantial augmentation in the power density of the cell in comparison to cell 1 and cell 2. The power density of the cell 3 is around 38% greater than that of the cell 1. In order to eliminate the effect of the cross-sectional area, cell 2 was constructed and analyzed. Though cell 2 and cell 3 have the same cross-sectional area of their flow channels, the power density of cell 3 was 32.6% greater than that of cell 2. In a study done by Paulino et al.(Paulino et al., 2017) a cell with the trapezoidal cross-sectional flow area resulted in low power density but better water management in comparison to the cell with square cross-sectional flow channel. It was concluded the reverse trapezoidal shape of the flow channel of the cell has pronounced impact on the cell's performance. It is reasoned that this might be due to the fact that the reverse trapezoidal shape brought about low gas flow rate in the cell's channels (see Figure 1 and Figure 3) and consequently allowed species to spend enough time for electrochemical reactions on the catalysts.

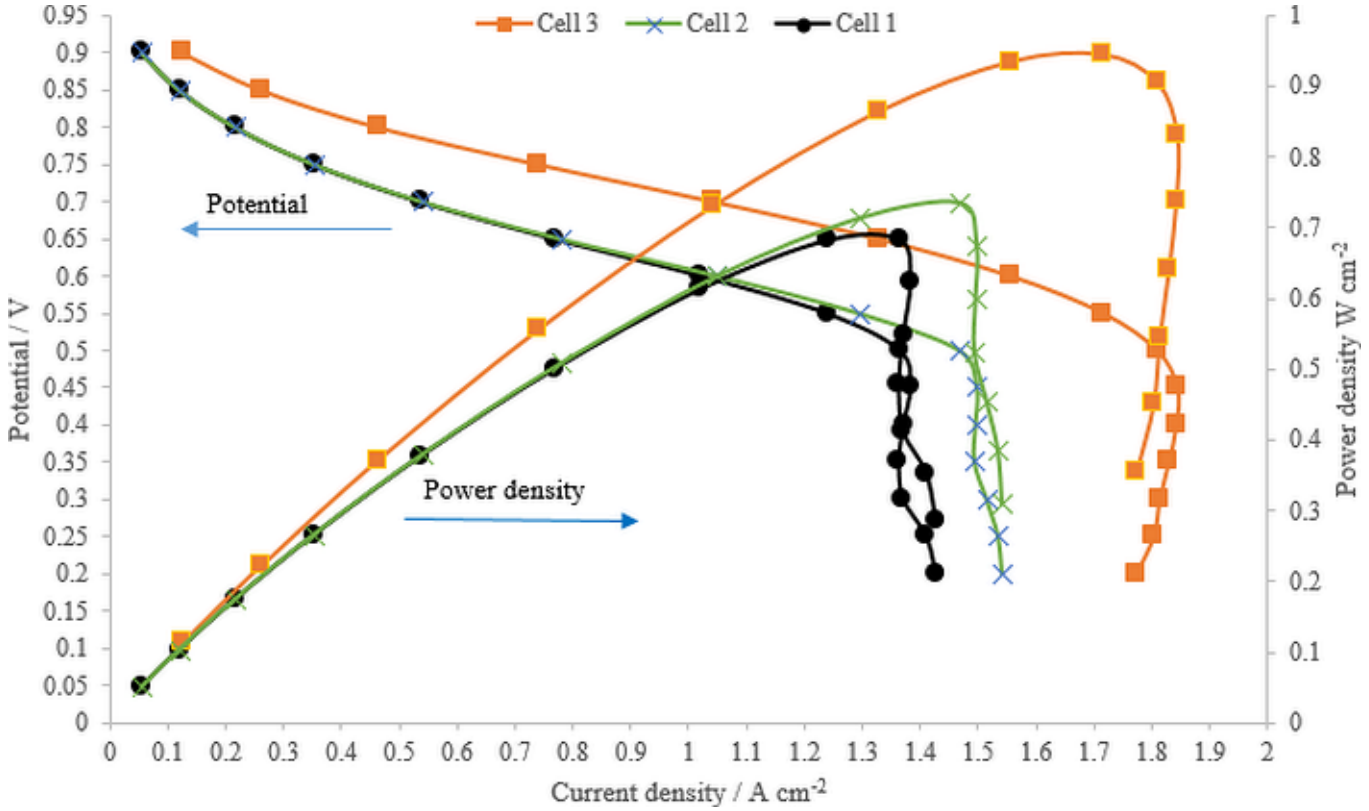


Figure 9. Polarization Curve of Cell 1, Cell 2 And Cell 3

CONCLUSION

In this work, a reverse trapezoidal cross-sectional shape for the bipolar plate of PEM fuel cells is investigated. This geometry increased cell performance by approximately 36 percent compared to a square cross-sectioned flow channel having channel width and height similar to the reverse trapezoid. Furthermore, for the same cross-sectional area, the single channel cell with reverse trapezoidal cross-sectional flow channel (cell 3) generated more than 32% power density compared to the cell with square cross-sectional flow channel (cell 2). However, the relative humidity obtained for this geometry turned out to be undesirably high. Therefore, this new geometry requires optimization with regards to its dimensions so as to obtain not only better cell performance but also effective water management concurrently.

DECLARATION OF ETHICAL STANDARDS

The author of this article declare that the materials and methods used in this study do not require ethical committee permission and/or legal-special permission.

CONFLICT OF INTEREST

There is no conflict of interest in this study.

REFERENCES

Arif, M., Cheung, S. C. P., & Andrews, J. (2022). Numerical investigation of effects of different flow channel configurations on the 100 cm^2 PEM fuel cell performance under different operating conditions. *Catalysis Today*, *397–399*(June), 449–462. https://doi.org/10.1016/j.cattod.2021.07.016

Arun Saco, S., Thundil Karuppa Raj, R., & Karthikeyan, P. (2016). A study on scaled up proton exchange membrane fuel cell with various flow channels for optimizing power output by effective water management using numerical technique. *Energy*, *113*, 558–573. https://doi.org/10.1016/j.energy.2016.07.079

Awan, A., Saleem, M., & Basit, A. (2018). Simulation of proton exchange membrane fuel cell by using ANSYS Fluent. *IOP Conference Series: Materials Science and Engineering*, *414*(1). https://doi.org/10.1088/1757-899X/414/1/012045

Carcadea, E., Ismail, M. S., Ingham, D. Bin, Patularu, L., Schitea, D., Marinoiu, A., … Varlam, M. (2021). Effects of geometrical dimensions of flow channels of a large-active-area PEM fuel cell: A CFD study. *International Journal of Hydrogen Energy*, *46*(25), 13572–13582. https://doi.org/10.1016/j.ijhydene.2020.08.150

Carcadea, E., Varlam, M., Ismail, M., Ingham, D. B., Marinoiu, A., Raceanu, M., … Ion-Ebrasu, D. (2020). PEM fuel cell performance improvement through numerical optimization of the parameters of the porous layers. *International Journal of Hydrogen Energy*, *45*(14), 7968–7980. https://doi.org/10.1016/j.ijhydene.2019.08.219

Ferng, Y. M., & Su, A. (2007). A three-dimensional full-cell CFD model used to investigate the effects of different flow channel designs on PEMFC performance. *International Journal of Hydrogen Energy*, *32*(17), 4466–4476. https://doi.org/10.1016/j.ijhydene.2007.05.012

Ibrahimoglu, B., Yilmazoglu, M. Z., & Celenk, S. (2017). Investigation of spiral flow-field design on the performance of a PEM Fuel Cell. *Fuel Cells*, *17*(6), 786–793. https://doi.org/10.1002/fuce.201700076

Jourdani, M., & Mounir, H. (2015). Temperature Distribution Effect on the Performance of PEM Fuel Cell Modeling and Simulation Using Ansys Fluent. *3rd International Renewable and Sustainable Energy Conference (IRSEC) Institute of Electrical and Elctronics Engineer (IEEE) DOI: 10.1109/IRSEC.2015.7455082.*

Kerkoub, Y., Benzaoui, A., Haddad, F., & Ziari, Y. K. (2018). Channel to rib width ratio influence with various flow field designs on performance of PEM fuel cell. *Energy Conversion and Management*, *174*(May), 260–275. https://doi.org/10.1016/j.enconman.2018.08.041

Li, C., Xu, X., Hu, H., Mei, N., & Yang, Y. (2021). Numerical investigation into the effect of serpentine flow channel with a variable cross-section on the performance of proton exchange membrane fuel cell. *International Journal of Energy Research*, *45*(5), 7719–7731. https://doi.org/10.1002/er.6352

Li, Y., Zhou, Z., Liu, X., & Wu, W. T. (2019). Modeling of PEM fuel cell with thin MEA under low humidity operating condition. *Applied Energy*, *242*(November 2018), 1513–1527. https://doi.org/10.1016/j.apenergy.2019.03.189

Lim, B. H., Majlan, E. H., Daud, W. R. W., Rosli, M. I., & Husaini, T. (2020). Numerical investigation of the effect of three-dimensional modified parallel flow field designs on proton exchange membrane fuel cell performance. *Chemical Engineering Science*, *217*, 115499. https://doi.org/10.1016/j.ces.2020.115499

Manso, A. P., Marzo, F. F., Mujika, M. G., Barranco, J., & Lorenzo, A. (2011). Numerical analysis of the influence of the channel cross-section aspect ratio on the performance of a PEM fuel cell with serpentine flow field design. *International Journal of Hydrogen Energy*, *36*(11), 6795–6808. https://doi.org/10.1016/j.ijhydene.2011.02.099

Paulino, A. L. R., Cunha, E. F., Robalinho, E., Linardi, M., Korkischko, I., & Santiago, E. I. (2017). CFD Analysis of PEMFC flow channel cross sections. *Fuel Cells*, *17*(1), 27–36. https://doi.org/10.1002/fuce.201600141

Penga, Ž., Tolj, I., & Barbir, F. (2016). Computational fluid dynamics study of PEM fuel cell performance for isothermal and non-uniform temperature boundary conditions. *International Journal of Hydrogen Energy*, *41*(39), 17585–17594. https://doi.org/10.1016/j.ijhydene.2016.07.092

Wang, X. D., Lu, G., Duan, Y. Y., & Lee, D. J. (2012). Numerical analysis on performances of polymer electrolyte membrane fuel cells with various cathode flow channel geometries. *International Journal of Hydrogen Energy*, *37*(20), 15778–15786. https://doi.org/10.1016/j.ijhydene.2012.04.028

Wang, Y., Ruiz Diaz, D. F., Chen, K. S., Wang, Z., & Adroher, X. C. (2020). Materials, technological status, and fundamentals of PEM fuel cells – A review. *Materials Today*, *32*(February), 178–203. https://doi.org/10.1016/j.mattod.2019.06.005

Wilberforce, T., El-Hassan, Z., Khatib, F. N., Al Makky, A., Mooney, J., Barouaji, A., … Olabi, A. G. (2017).

Development of Bi-polar plate design of PEM fuel cell using CFD techniques. *International Journal of Hydrogen Energy*, *42*(40), 25663–25685. https://doi.org/10.1016/j.ijhydene.2017.08.093

Wilberforce, T., Ijaodola, O., Khatib, F. N., Ogungbemi, E. O., El Hassan, Z., Thompson, J., & Olabi, A. G. (2019). Effect of humidification of reactive gases on the performance of a proton exchange membrane fuel cell. *Science of the Total Environment*, *688*, 1016–1035. https://doi.org/10.1016/j.scitotenv.2019.06.397

Yi, J. S., & Van Nguyen, T. (1999). Multicomponent Transport in porous electrodes of proton exchange membrane fuel cells using the ınterdigitated gas distributors. *Journal of The Electrochemical Society*, *146*(1), 38–45. https://doi.org/10.1149/1.1391561

Zhao, J., & Li, X. (2019). A review of polymer electrolyte membrane fuel cell durability for vehicular applications: Degradation modes and experimental techniques. *Energy Conversion and Management*, *199*(September 2019), 112022. https://doi.org/10.1016/j.enconman.2019.112022